Vibrational spectroscopy of $NO^+(H_2O)_n$: Evidence for the intracluster reaction $NO^+(H_2O)_n \rightarrow H_3O^+(H_2O)_{n-2}$ (HONO) at $n \geq 4$

Jong-Ho Choi, Keith T. Kuwata, Bernd-Michael Haas, Yibin Cao, Matthew S. Johnson, and Mitchio Okumura[a)]

Arthur Amos Noyes Laboratory of Chemical Physics,[b)] California Institute of Technology, Pasadena, California 91125

(Received 3 January 1994; accepted 7 February 1994)

Infrared spectra of mass-selected clusters $NO^+(H_2O)_n$ for $n=1$ to 5 were recorded from 2700 to 3800 cm^{-1} by vibrational predissociation spectroscopy. Vibrational frequencies and intensities were also calculated for $n=1$ and 2 at the second-order Møller–Plesset (MP2) level, to aid in the interpretation of the spectra, and at the singles and doubles coupled cluster (CCSD) level energies of $n=1$ isomers were computed at the MP2 geometries. The smaller clusters ($n=1$ to 3) were complexes of H_2O ligands bound to a nitrosonium ion NO^+ core. They possessed perturbed H_2O stretch bands and dissociated by loss of H_2O. The H_2O antisymmetric stretch was absent in $n=1$ and gradually increased in intensity with n. In the $n=4$ clusters, we found evidence for the beginning of a second solvation shell as well as the onset of an intracluster reaction that formed HONO. These clusters exhibited additional weak, broad bands between 3200 and 3400 cm^{-1} and two new minor photodissociation channels, loss of HONO and loss of two H_2O molecules. The reaction appeared to go to completion within the $n=5$ clusters. The primary dissociation channel was loss of HONO, and seven vibrational bands were observed. From an analysis of the spectrum, we concluded that the $n=5$ cluster rearranged to form $H_3O^+(H_2O)_3$(HONO), i.e., an adduct of the reaction products.

I. INTRODUCTION

The nitrosonium ion NO^+ and its hydrates play an important role in the ion chemistry of Earth's upper atmosphere.[1] The NO radical possesses a low ionization potential (9.26 eV) and is thus readily ionized by either photoionization or charge transfer. NO^+ is the major primary ion in the D region of the ionosphere, where it is formed by solar Lyman-α radiation. However, measurements of the positive ion composition in the ionosphere, beginning with rocket-borne mass-spectrometric observations by Narcisi and Bailey,[2] have revealed that the predominant ionic species in the D region are the hydronium ion hydrates, $H_3O^+(H_2O)_n$. The conversion of NO^+ to $H_3O^+(H_2O)_n$ is now known to occur by a hydration mechanism.[3,4] NO^+ first undergoes a sequence of solvation steps to form a hydrated cluster ion, $NO^+(H_2O)_3$. This cluster subsequently reacts with another water molecule:

$$NO^+(H_2O)_3 + H_2O \rightarrow H_3O^+(H_2O)_2 + HONO \qquad (1)$$

to form the hydrated hydronium ions.

Gas-phase experiments on hydrated NO^+ clusters have examined the association kinetics and thermochemistry in order to understand the processes occurring in the ionosphere. Several groups used stationary[4,5] and flowing afterglow techniques[6,7] to measure the rate constants of the successive hydration steps and the final reaction (1). Puckett and Lineberger[8] identified the neutral product HONO in their stationary afterglow apparatus from their negative ion mass spectrum. French *et al.*[9] studied the kinetics and equilibria of NO^+ hydration by pulsed high-pressure mass spectrometry. They obtained hydration enthalpies of $\Delta H^\circ_{0,1} = -18.5 \pm 1.5$ kcal mol^{-1} for NO^+ and $\Delta H^\circ_{1,2} = -16.1 \pm 1.0$ kcal mol^{-1} for $NO^+(H_2O)$. They extrapolated these values to estimate $\Delta H^\circ_{2,3} = -13.5 \pm 1.0$ kcal mol^{-1}. Burdett and Hayhurst[10] found a similar value for the hydration of NO^+ of $\Delta H^\circ_{0,1} = -19.3 \pm 2.4$ kcal mol^{-1} in their studies of boundary layer cooling of ions sampled from flames.

In aqueous solution, NO^+ is a key intermediate in the nitrosation reactions of organic compounds.[11] Studies of nitrosation reactions have established that the mechanism depends on acidity. Both NO^+ and protonated nitrous acid are thought to participate in the rate-determining step at high acidity ($pH \leq 1$). Protonated nitrous acid, $H_2NO_2^+$ (nitrosohydronium or nitrous acidium ion), is believed to exist as a weakly bound complex of NO^+ and H_2O, depicted in Fig. 1(a), in equilibrium with NO^+:

$$H^+ + HONO \leftrightarrow NO^+(H_2O) \leftrightarrow NO^+ + H_2O. \qquad (2)$$

The equilibrium constants are not accurately known and there has been no direct detection of $NO^+(H_2O)$ in the condensed phase.

Several theoretical calculations[12–17] have examined the optimized geometries of protonated nitrous acid, although no theoretical studies of the higher hydrates of NO^+ have been performed. The consensus is that the most stable form is an ion–molecule complex between NO^+ and H_2O, rather than a purely covalently bound cation. De Petris *et al.*[17] performed *ab initio* calculations that included electron correlation and predicted that protonated nitrous acid has six different isomers which are true minima on the potential energy hypersurface. For the lowest-energy form, $NO^+(H_2O)$, they obtained an enthalpy of formation $\Delta H^\circ_f = 160 \pm 2$ kcal mol^{-1}, in good agreement with the experimental value of 159.0 ± 1.5 kcal mol^{-1} based on the binding energy[9] of $NO^+(H_2O)$.

[a)]Author to whom correspondence should be addressed.
[b)]Contribution No. 8900.

 0021-9606/94/100(10)/7153/13/$6.00

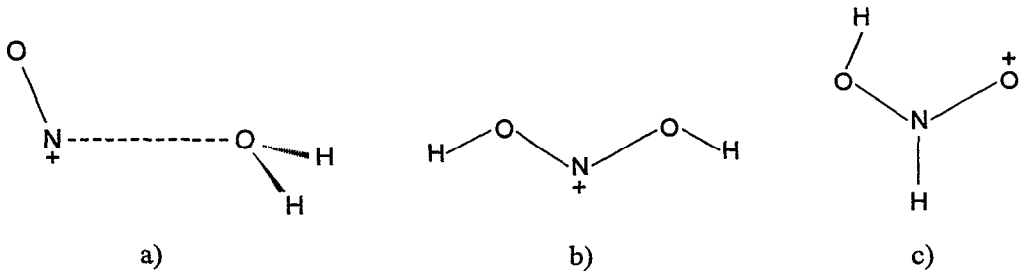

FIG. 1. Isomers of protonated nitrous acid. The geometry of the most stable structure predicted at the MP2/6-31G** level is (a) $NO^+(H_2O)$, while (b) $HONOH^+$ and (c) $HON(H)O^+$ are potential energy minima lying at higher energies.

They found that the next lowest-energy isomers are formed by protonating either the terminal oxygen to form $N(OH)_2^+$, or the nitrogen atom to form $HON(H)O^+$, isomers shown in Fig. 1. Both structures were calculated to have ΔH_f° over 41 kcal mol^{-1} higher than that of the $NO^+(H_2O)$ complex. Such energetic metastable isomers have not been observed experimentally.

If the complex $NO^+(H_2O)$ is the lowest-energy isomer of protonated nitrous acid, the proton affinity of HONO is PA=187.7 kcal mol^{-1},[9] 11 kcal mol^{-1} higher than that of H_2O. Direct protonation of nitrous acid has not been observed in the gas phase because of the difficulty in generating pure HONO. Using collisionally activated dissociation (CAD) mass spectrometry, De Petris *et al.*[17] found that only one isomer of protonated nitrous acid is produced in proton transfer reactions such as $H_3^+ + CH_3ONO$. They presented circumstantial evidence that this isomer is the complex $NO^+(H_2O)$. However, they observed no metastable signal and thus were unable to glean further structural information on protonated nitrous acid from kinetic energy release measurements.

Basic thermodynamic and kinetic data have been measured for reaction (1), but little is known about the mechanism and the role of the solvent H_2O in assisting the reaction. The reaction is estimated to be slightly endothermic ($\sim+2$ kcal mol^{-1}).[9,18] The rate constant[4–7] was found to be $k \approx 7\times10^{-11}$ cm^3 s^{-1}, based on the disappearance of the $NO^+(H_2O)_3$ cluster. The production of $H_3O^+(H_2O)_2$ was inferred rather than directly measured because the hydronium ion hydrates equilibrated too rapidly. In speculating about the molecular mechanism of reaction (1), Fehsenfeld *et al.*[6] postulated intermediate cluster configurations in which not all H_2O moieties solvated the NO^+, but conventional mass-spectrometric and kinetic experiments have shed no further light on their key idea, that the reaction requires solvent reorganization within an activated cluster.

IR photodissociation spectroscopy coupled with tandem mass spectrometry has proven to be a powerful method for investigating cluster ions.[19–22] We have recently investigated similar intracluster reactions in hydrated nitronium ion clusters $NO_2^+(H_2O)_n$ using the technique of vibrational predissociation spectroscopy.[23,24] In these experiments, the infrared spectra of mass-selected ions are obtained by detecting photofragment ions as a function of laser frequency. We observed a dramatic change in the vibrational spectrum and dissociation branching ratio of the NO_2^+ hydrate clusters at a critical cluster size, indicative of an intracluster reaction.

In this paper, we describe our investigations of the vibrational predissociation spectroscopy of the hydrated clusters of the nitrosonium ion, $NO^+(H_2O)_n$. We report infrared spectra and photofragment yields for $n=1$–5. We have also performed *ab initio* calculations of the vibrational frequencies and intensities of the clusters $n=1$ and 2 to confirm our vibrational assignments. Our calculations were undertaken because there were no published theoretical estimates of the vibrational frequencies for $n=1$, nor of the structure, energetics, and vibrational frequencies for $n=2$.

II. EXPERIMENT

The apparatus employed in these experiments[20,23] will be described in detail elsewhere,[24] and only a brief account will be presented here. $NO^+(H_2O)_n$ ($n=1$ to 5) clusters were generated by a high-pressure, pulsed discharge source. An MKS mass-flow controller was used to produce a mixture of 12% NO (Matheson Gas Co. purity 99%) seeded in ultrahigh purity (99.999%) H_2 or He. Hydrate clusters could be readily formed using only the trace water vapor already present in the stainless-steel inlet line. The pressure was 1000 Torr at room temperature in the stagnation volume of a piezo-driven pulsed valve. Gas was pulsed (200 μs width) at a repetition rate of 10 Hz into a 1 mm diameter, 1.5 cm long channel and expanded into the first differential vacuum chamber maintained at 2 to 5×10^{-5} Torr by a 10 in. diffusion pump. A discharge was struck as the gas flowed through the channel by applying a high voltage pulse (-1.5 to -3 kV, 100 μs wide) between two electrodes near the entrance. The ions formed in the plasma were thermalized as the gas flowed through the channel and further cooled in the supersonic expansion. The expanding plasma was skimmed and entered a second region (6 in. diffusion pump, 1×10^{-6} Torr) containing the time-of-flight ion optics. The ions were extracted by a pulsed electric field 15 μs in duration and accelerated to 1.3 kV, focused by a pair of einzel lenses. The ions passed through an additional stage of differential pumping (4 in. diffusion pump, 1×10^{-6} Torr) and entered the photolysis chamber (500 L/s turbomolecular pump, 3×10^{-7} Torr).

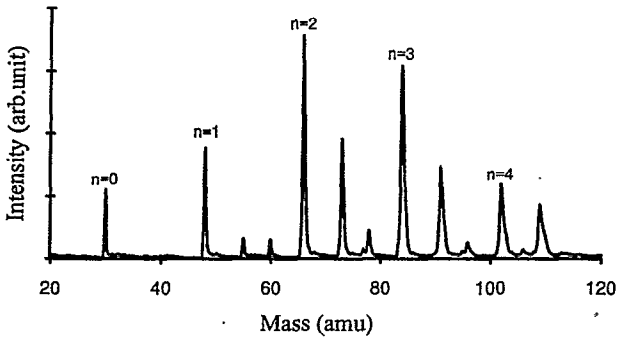

FIG. 2. Time-of-flight mass spectrum of hydrated nitrosonium clusters (n =0–4). The ions were formed in a glow discharge of 12% NO seeded in ultrahigh purity H_2 at 1000 Torr. The formation of hydrates is due to the presence of a trace of H_2O vapor.

Parent ions of a specific mass were selected by a 1 cm long mass gate which rejected all ions of other m/e. The ions were vibrationally excited by a collimated infrared beam, which was generated by a pulsed $LiNbO_3$ optical parametric oscillator[25] (OPO) and timed to intersect the selected ions at the spatial focus of the time-of-flight mass spectrometer. The OPO was pumped by a Quanta Ray GCR 12S Nd:YAG laser whose 1.06 μm output was propagated 3 m to achieve a nominally Gaussian transverse mode at the input of the OPO. The OPO was tunable from 2700 to 6700 cm^{-1} by simultaneously adjusting the crystal and grating angles. Typical OPO pulse energies were about 3 to 5 mJ with a linewidth of 1.5 cm^{-1}. The laser beam path from the OPO to the vacuum chamber was purged with dry air to eliminate absorption by water vapor.

The fragment ions resulting from IR excitation were separated from the parent ions using a reflectron energy analyzer, and then detected by a microchannel plate detector. The signal was preamplified and then collected by a transient digitizer. Predissociation spectra were obtained by stepping the OPO wavelength and averaging the photofragment ion signal for 200 shots at each wavelength. Fragment ion background arising from dissociation of metastable parents was subtracted to obtain the fragment signal due solely to photodissociation. The data were then normalized with respect to the OPO pulse energy. Between 2 and 14 such scans were averaged, depending on the photofragment signal intensity. The OPO laser wavelength was calibrated during the scan by simultaneously recording the rovibrational spectra of either methane or hydrogen chloride in a photoacoustic cell.

III. EXPERIMENTAL RESULTS

A typical time-of-flight mass spectrum of nitrosonium ion hydrate clusters is shown in Fig. 2. While this distribution peaked at $NO^+(H_2O)_2$, it could be shifted by varying the stagnation temperature and pressure, source voltage, and pulsed valve settings. Two additional series of hydrates can be seen in Fig. 2, $H_3O^+(H_2O)_n$ and, very weakly, $(NO)_2^+(H_2O)_n$. The relative intensities of these species also varied, but did not interfere with the measurements reported here.

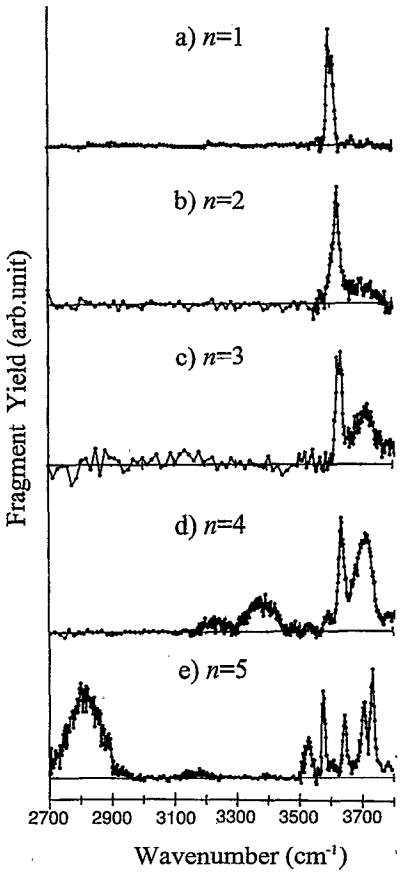

FIG. 3. Vibrational predissociation spectra of $NO^+(H_2O)_n$ (n=1–5). The photofragment ions detected were $NO^+(H_2O)_{n-1}$ (n=1–4) and $H_3O^+(H_2O)_3$ (n=5), respectively.

We recorded infrared spectra of mass-selected clusters $NO^+(H_2O)_n$ for n=1–5 in the 2700–3800 cm^{-1} region. Figure 3 presents the infrared spectra for n=1–5 over the entire frequency range and Table I lists the observed band maxima.

A. Photodissociation behavior

The only photofragment ions detected upon infrared excitation of the clusters $NO^+(H_2O)_n$ (n=1 to 3) were $NO^+(H_2O)_{n-1}$, indicating that a single water molecule evaporated upon vibrational excitation:

$$NO^+(H_2O)_n \rightarrow NO^+(H_2O)_{n-1} + H_2O, \quad n=1-3. \qquad (3)$$

Figure 4 shows the dependence of the photodissociation signal on laser pulse energy for these three clusters when exciting the band observed at ~3620 cm^{-1}. The dissociation signal for n=1 exhibited a quadratic dependence, as seen from the linear dependence of the square root of the signal plotted against laser pulse energy in Fig. 4(a). The dissociation of n=1 clusters thus involved two-photon excitation. The rollover at high fluence probably resulted from saturation. In the case of n=2, the fragment ion signal showed both linear and nonlinear behavior depending on source conditions. In Fig. 4(b), the signal was a sum of linear and quadratic terms, since the plot of the square root of signal vs pulse energy

TABLE I. Observed vibrational frequencies of $NO^+(H_2O)_n$ ion clusters.

Cluster	Frequency (cm^{-1})	Assignment
$NO^+(H_2O)$	3599, 3611	H_2O sym. stretch
$NO^+(H_2O)_2$	3622	H_2O sym. stretch
	3695	H_2O antisym. stretch
$NO^+(H_2O)_3$	3630	H_2O sym. stretch
	3712	H_2O antisym. stretch
$NO^+(H_2O)_4$ [a]	3230	H-bonded OH stretch
	3375	H-bonded OH stretch
	3635	H_2O sym. stretch
	3713	H_2O antisym. stretch
$NO^+(H_2O)_5$	2800	H-bonded H_3O^+ stretch
	3190	H-bonded H_3O^+ stretch
	3530	H-bonded H_2O donor OH stretch
	3576	HONO OH stretch
	3644	H_2O sym. stretch
	3710	H-bonded H_2O free OH stretch
	3734	H_2O antisym. stretch
H_2O monomer[b]	3657	sym. stretch, ν_1
	3756	antisym. stretch, ν_3
HONO (*trans*) monomer[c]	3591	OH stretch
HONO (*cis*) monomer[c]	3426	OH stretch

[a]Band assignments are based on the structure of Fig. 7(c).
[b]Reference 33.
[c]Reference 28.

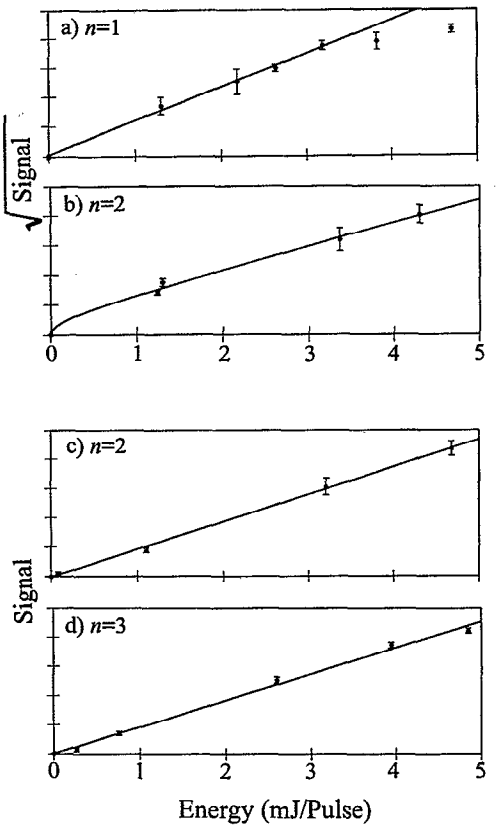

FIG. 4. The dependence on laser pulse energy of the fragment signal from photodissociation of the parent ions $NO^+(H_2O)_n$ ($n=1$–3) excited in the H_2O symmetric stretch. In the upper two panels, the square root of the photodissociation signal is plotted for (a) $n=1$ and (b) $n=2$. The curves are fit to a sum of linear and quadratic terms. In the lower two panels, the photodissociation signal is plotted directly for (c) $n=2$ and (d) $n=3$.

approached a straight line only at higher energies. Under alternate source conditions, shown in Fig. 4(c), the signal depended linearly on the pulse energy. The detected signal for $n=3$ depended linearly on laser power as shown in Fig. 4(d), indicating that the predissociation of this cluster was a single photon process.

Infrared excitation of the $n=4$ cluster produced photofragments at three masses, corresponding to $NO^+(H_2O)_3$, $NO^+(H_2O)_2$, and $H^+(H_2O)_3$. Thus, the following photodissociation processes were competing:

$$NO^+(H_2O)_4 \rightarrow NO^+(H_2O)_3 + H_2O, \quad (4a)$$

$$\rightarrow NO^+(H_2O)_2 + 2H_2O, \quad (4b)$$

$$\rightarrow H_3O^+(H_2O)_2 + HONO. \quad (4c)$$

The major dissociation channel was loss of one water, channel (4a). The minor $NO^+(H_2O)_2$ product in Eq. (4b) is likely due to evaporation of a neutral water dimer $(H_2O)_2$, although an alternative is the secondary spontaneous dissociation of the primary product ion in channel (4a), a process which requires more energy. The observation of channel (4c) signaled the onset of a new dissociation channel, loss of a nitrous acid molecule. The relative yields were wavelength dependent. When exciting absorption bands observed in the 3600–3800 cm^{-1} region, the branching ratio of channels (4a), (4b), and (4c) was 8:1.5:1. Contributions from channels (4b) and (4c) were negligible when exciting bands in the 3400 cm^{-1} region.

There was a significant change in the photofragmentation pattern of the $n=5$ cluster, $NO^+(H_2O)_5$. We detected photofragments at three masses: $H^+(H_2O)_4$, $H^+(H_2O)_3$, and $NO^+(H_2O)_4$. The dominant channel throughout the observed spectral region was

$$NO^+(H_2O)_5 \rightarrow H_3O^+(H_2O)_3 + HONO. \quad (5)$$

Thus, unlike the smaller clusters, infrared excitation of $n=5$ led almost exclusively to loss of neutral nitrous acid.

B. Vibrational predissociation spectra

The infrared spectrum of protonated nitrous acid ($n=1$) exhibited a single vibrational band in the 2700–3800 cm^{-1} range [Fig. 3(a)]. This band was only 50 cm^{-1} lower in frequency than the symmetric stretch of the water monomer (Table I). Closer examination revealed that the band was a doublet with maxima at 3599 and 3611 cm^{-1}, as seen in Fig. 5(a).

The clusters $NO^+(H_2O)_n$ ($n=2$ and 3) had two absorption bands in the 2700–3800 cm^{-1} region [Figs. 3(b) and 3(c), Table I]. The lower frequency bands at ~3630 cm^{-1} were sharp and resembled in shape and position the band observed for $NO^+(H_2O)$. The higher frequency bands at ~3700 cm^{-1} were broad. Based on the proximity of these bands to the H_2O monomer stretch frequencies,[26] we assigned these bands to the symmetric and antisymmetric stretch modes of water ligands, respectively.

The spectrum of $n=4$, shown in Fig. 3(d), consisted of four bands. Two bands at 3635 and 3713 cm^{-1} were similar

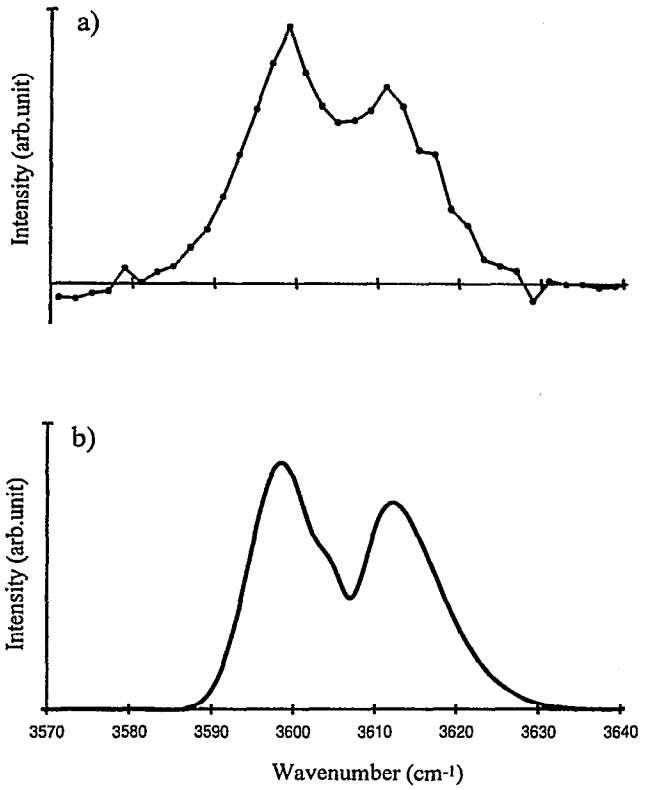

FIG. 5. (a) Detail of the 3605 cm^{-1} band from the vibrational predissociation of $NO^+(H_2O)$. The ordinate is the yield of photofragment ions NO^+. (b) Simulation of the rotational band contour using rotational constants calculated from the *ab initio* structure of $NO^+(H_2O)$. Upper and lower state differences and centrifugal distortion constants were estimated from those of *t*-HONO. The predicted asymmetric rotor spectrum used a rotational temperature of 120 K and was convoluted with a resolution linewidth of 1.5 cm^{-1}.

to the bands observed in $n \leqslant 3$, while two new bands at 3230 and 3375 cm^{-1} were substantially broader. The two high-frequency bands were assigned to H_2O symmetric and antisymmetric stretches, respectively. The two lower frequency bands were broad and significantly red-shifted relative to the other OH bands, indicative of an OH bond involved as a donor in hydrogen bonding.

The spectrum of the $n=5$ cluster was qualitatively different from those of the smaller clusters. The infrared absorption spectrum of the $NO^+(H_2O)_5$ cluster shown in Fig. 3(e) possessed seven distinct bands, two in the 2700–3200 cm^{-1} region, and five others in the 3500–3800 cm^{-1} region.

The strongest band, at 2800 cm^{-1}, was broad and had the appearance of the stretching band of an ionic OH group participating as a donor in hydrogen bonding. Such bands were first observed in $H_3O^+(H_2O)_n$ clusters by Schwarz.[27] Lee and co-workers[19] in their studies of $H_3O^+(H_2O)_n$ clusters and Cao *et al.*[23] in their studies of $NO_2^+(H_2O)_n$ observed similar bands and assigned them to the hydrogen-bonded OH antisymmetric stretch of the H_3O^+ ion. In general, these vibrations occurred below 2700 cm^{-1} unless the hydronium ion was fully solvated. We therefore concluded that the $n=5$ clusters possessed a hydronium ion core, with ligands bonded to all three OH bonds.

The strong H_3O^+ band is often accompanied by a broad but weaker band at higher frequency. We assigned the weaker 3190 cm^{-1} band as this companion mode. The exact assignment of such bands (symmetric stretch of H_3O^+, bending overtone, combination band) is still a matter of uncertainty.[19,27]

The five higher-frequency bands of the $n=5$ spectrum can be assigned as OH stretches of the ligands bound to the H_3O^+ core. One of the two bands near the OH stretching frequency of the *trans* nitrous acid monomer[28,29] (3591 cm^{-1}) could be assigned to the free OH stretch of HONO; the remaining bands we assigned to H_2O. Detailed assignments based on a proposed structure will be discussed below.

IV. *AB INITIO* CALCULATIONS ON THE $n=1$ AND $n=2$ CLUSTERS

A. Computational approach

To help interpret the predissociation spectra of the $n=1$ and $n=2$ clusters, we performed *ab initio* calculations at the Hartree–Fock (HF) and the second-order Møller–Plesset[30] (MP2) level using the 6-31G** basis set[31] to compute geometries and vibrational frequencies. Single point energies were also computed at the coupled cluster with single and double excitations (CCSD) level of theory using the 6-31G** basis set for $n=2$, and the 6-311G($2df$,$2pd$) basis set for $n=1$ and its isomers (see Table II). All electrons were correlated at the MP2 level, but core electrons were frozen at the CCSD level. Calculations were done using the GAUSSIAN 92 system of programs[32] on a Cray Y-MP supercomputer.

The geometries of $NO^+(H_2O)$, $N(OH)_2^+$, and $HON(H)O^+$ were optimized at the MP2/6-31G** level using the geometries of De Petris *et al.*[17] as the initial guesses. We found substantially the same results as De Petris *et al.* for all three isomers. Harmonic vibrational frequencies and infrared intensities for $NO^+(H_2O)$, $N(OH)_2^+$, and $HON(H)O^+$ (Tables

TABLE II. *Ab initio* relative stabilities for $H_2NO_2^+$ isomers. MP2 calculations use the 6-31G** basis set. CCSD calculations use the 6-311G($2df$,$2pd$) basis set.

	ΔE_0 (kcal mol^{-1})				$\Delta H^0_{298.15}$ (kcal mol^{-1})	
Cluster	MP2	MP2+ZPE	CCSD	CCSD+ZPE[a]	MP2	CCSD[a]
$NO^+(H_2O)$	0	0	0	0	0	0
$HON(H)O^+$	37.8	40.8	32.8	35.8	39.6	34.6
$N(OH)_2^+$	38.3	41.2	29.7	32.7	40.1	31.5

[a]Using the MP2 harmonic vibrational frequencies.

TABLE III. *Ab initio* harmonic frequencies (MP2/6-31G**) for $NO^+(H_2O)$.

Mode	Approx. description	Frequencies (cm^{-1}) [Intensities (km mol^{-1})]
$\omega_1(a')$	O–H sym. stretch	3820(196)
$\omega_2(a')$	N–O stretch	2099(92)
$\omega_3(a')$	H_2O bend	1682(65)
$\omega_4(a')$	H_2O wag	472(272)
$\omega_5(a')$	N···O stretch	281(101)
$\omega_6(a')$	O–N···O bend	248(10)
$\omega_7(a'')$	O–H antisym. stretch	3942(159)
$\omega_8(a'')$	H_2O rock	470(56)
$\omega_9(a'')$	H_2O twist	116(36)

TABLE V. *Ab initio* harmonic frequencies (MP2/6-31G**) for $HON(H)O^+$.

Mode	Approx. description	Frequencies (cm^{-1}) [Intensities (km mol^{-1})]
$\omega_1(a')$	O–H stretch	3550(320)
$\omega_2(a')$	N–H stretch	3355(135)
$\omega_3(a')$	N–O stretch	1656(159)
$\omega_4(a')$	ONH bend+N–O stretch	1509(83)
$\omega_5(a')$	HON bend+N–O stretch	1430(9)
$\omega_6(a')$	ONH bend+N–O stretch	1239(215)
$\omega_7(a')$	ONO ip bend	668(53)
$\omega_8(a'')$	ON(H)O umbrella	1065(110)
$\omega_9(a'')$	ONO op bend	752(181)

III, IV, and V) were then determined using analytic second derivatives. All frequencies found were real, which confirmed that the optimized structures obtained were true minima of the potential energy hypersurface.

There has apparently been no previous theoretical work on the $n=2$ clusters. For our calculations, then, we assumed that the isomer of interest would be of the form $NO^+(H_2O)_2$, with at least C_s and perhaps C_{2v} symmetry. The structure was fully optimized under these symmetry constraints at both the HF and the MP2 levels. In addition, due to the presence of several low-frequency (<200 cm^{-1}) modes, it was necessary to use more stringent convergence criteria. The minimum calculated was converged to an rms force of less than 1×10^{-5} a.u. and to an rms displacement of 4×10^{-5} a.u. Both the HF and MP2 structures had C_s symmetry, although the HF structure was nearly C_{2v}. Harmonic vibrational frequencies (Table VI) showed that both the HF and the MP2 optimized structures were potential energy minima.

In order to relate the *ab initio* frequencies to experimental values, we also computed the vibrational frequencies of H_2O at the MP2/6-31G** level. We obtained scaling factors by comparing the computed values of 3894 (a_1) and 4032 cm^{-1} (b_2) with the experimental values of 3657 (a_1) and 3756 cm^{-1} (b_2).

To estimate the binding energies and enthalpies of $NO^+(H_2O)_n$ ($n=1$ and 2), CCSD/6-311G($2df$,$2pd$) energies were calculated for $NO^+(H_2O)_2$, $NO^+(H_2O)$, NO^+, and H_2O at their MP2 optimized geometries. Because both the MP2 and CCSD levels of theory are size-consistent, binding energies may be calculated simply as the sum and difference of the appropriate electronic energies. Corrections for zero-point vibrational energy were made to both the MP2 and CCSD energies using the MP2 level vibrational frequencies. Finally, binding enthalpies at 298.15 K were also estimated using the MP2 frequencies. Our enthalpy corrections differ from those of Ref. 17. Results are listed in Table VII.

TABLE IV. *Ab initio* harmonic frequencies (MP2/6-31G**) for $N(OH)_2^+$.

Mode	Approx. description	Frequencies (cm^{-1}) [Intensities (km mol^{-1})]
$\omega_1(a_1)$	O–H sym. stretch	3610(105)
$\omega_2(a_1)$	N–O sym. stretch+NOH bend	1539(77)
$\omega_3(a_1)$	N–O sym. stretch	1280(22)
$\omega_4(a_1)$	ONO bend	713(20)
$\omega_5(a_2)$	ONO shear	760(0)
$\omega_6(b_1)$	NOH shear	875(291)
$\omega_7(b_2)$	O–H antisym. stretch	3583(848)
$\omega_8(b_2)$	N–O antisym. str.+NOH bend	1560(115)
$\omega_9(b_2)$	N–O antisym. str.+ONO shear	1293(439)

B. $NO^+(H_2O)$ and its isomers

The optimized geometry of $NO^+(H_2O)$ obtained at the MP2/6-31G** level is essentially identical to that obtained by De Petris *et al.*[17] As shown in Fig. 1(a), the oxygen atom of the water binds to the nitrogen end of the cation, which carries ~70% of the charge; the N···O separation is 2.202 Å, and the O=N···O bond angle is 100.2°. The geometries of the NO^+ and H_2O moieties do not differ significantly from those of free NO^+ and H_2O.

The binding enthalpy at the CCSD/6-311G $\times(2df,2pd)$//MP2/6-31G** level is $\Delta H^\circ_{298}=20.9$ kcal mol^{-1} (see Table VII), slightly higher than the experimental enthalpy of 18.5 kcal mol^{-1}.[9] The scaled MP2 frequencies of the H_2O vibrations are 3587 cm^{-1} for the symmetric stretch and 3671 cm^{-1} for the antisymmetric stretch, and the band strengths are comparable.

TABLE VI. *Ab initio* harmonic frequencies for $NO^+(H_2O)_2$.

Mode	Approx. description	Frequencies (cm^{-1}) [intensities (km mol^{-1})] RHF/6-31G**	MP2/6-31G**
$\omega_1(a')$	O–H antisym. stretch	4213(292)	3978(180)
$\omega_2(a')$	O–H sym. stretch	4114(14)	3859(75)
$\omega_3(a')$	N–O stretch	2800(101)	2097(36)
$\omega_4(a')$	H_2O bend	1794(20)	1698(82)
$\omega_5(a')$	H_2O rock	425(165)	423(126)
$\omega_6(a')$	H_2O wag	378(764)	397(482)
$\omega_7(a')$	N···O sym. stretch	202(2)	254(52)
$\omega_8(a')$	N···OH bend	27(0)	201(14)
$\omega_9(a')$	H_2O twist	65(6)	105(22)
$\omega_{10}(a')$	O···N···O bend	85(0)	33(0)
$\omega_{11}(a'')$	O–H antisym. stretch	4213(32)	3977(66)
$\omega_{12}(a'')$	O–H sym. stretch	4112(179)	3857(132)
$\omega_{13}(a'')$	H_2O bend	1793(194)	1693(69)
$\omega_{14}(a'')$	H_2O wag	360(0)	379(118)
$\omega_{15}(a'')$	H_2O rock	414(56)	375(84)
$\omega_{16}(a'')$	N···O antisym. stretch	238(23)	224(4)
$\omega_{17}(a'')$	N···OH bend	318(41)	207(1)
$\omega_{18}(a'')$	H_2O op twist	28(0)	26(7)

TABLE VII. *Ab initio* thermochemical data for $NO^+(H_2O)_n \rightarrow NO^+(H_2O)_{n-1}+H_2O$.

Cluster	ΔE_0 (kcal mol^{-1})						ΔH^0_{298} (kcal mol^{-1})			
	MP2 6-31G**	MP2+ZPE 6-31G**	CCSD 6-31G**	CCSD+ZPE[a] 6-31G**	CCSD EXT[b]	CCSD+ZPE[a] EXT[b]	MP2 6-31G**	CCSD[a] 6-31G**	CCSD[a] EXT[b]	Expt.
$n=1$	25.1	23.1	23.9	21.9	22.2	20.2	23.8	22.6	20.9	18.5[c] 19.3[d]
$n=2$	19.5	18.0	18.9	17.4			18.0	17.5		16.1[c]

[a]Using the MP2/6-311G** harmonic vibrational frequencies.
[b]EXT refers to the 6-311G(2*df*,2*pd*) basis set.
[c]Reference 9.
[d]Reference 10.

Two higher lying isomers formed by protonation of alternate sites were also computed at the CCSD/6-311G(2*df*,2*pd*)//MP2/6-31G** level. The "W" shaped isomer, $HONOH^+$, shown in Fig. 1(b), had an enthalpy $\Delta H^\circ_{298}=31.5$ kcal mol^{-1} above that of the $NO^+(H_2O)$ isomer. The enthalpy of the $HON(H)O^+$ isomer, formed by protonating the nitrogen atom of *cis* HONO, was $\Delta H^\circ_{298}=34.6$ kcal mol^{-1} above the cluster isomer. These energies are somewhat lower than the values of 41.5 and 41.7 kcal mol^{-1} calculated by De Petris *et al.*[17] at the MP4/6-311G** level. Both of these isomers possessed strong X–H (X=N, O) absorption bands, but the scaled vibrational frequencies all were below 3500 cm^{-1} (see Tables IV and V).

C. $NO^+(H_2O)_2$

Figure 6 shows the optimized C_s geometry obtained for the minimum energy structure of $NO^+(H_2O)_2$ at the MP2/6-31G** level. The H_2O molecules both bind to the nitrogen atom. The ion–solvent bond lengths are 2.318 Å and, at this level of theory, the O···N···O angle is 109.9°. The NO bond is predicted to be only 5.9° from perpendicular with respect to the O···N···O plane. The dipole–dipole interaction between the H_2O molecules at the computed geometry is repulsive. This effect alone would favor by 0.5 kcal mol^{-1} having the H_2O on opposing sides of the nitrogen atom. However, at the MP2 level, this latter geometry (C_{2v} symmetry, with the H_2O molecules on opposite sides and the O···N···O angle close to 180°) is 0.5 kcal mol^{-1} higher in energy; thus, the weak dipole repulsion is offset by other factors. The low frequency of the O···N···O bend, 33 cm^{-1}, indicates that the potential energy surface is flat along this coordinate. The equilibrium O···N···O bond angle, calculated with this basis set and constrained to C_s symmetry, should therefore be treated with caution.

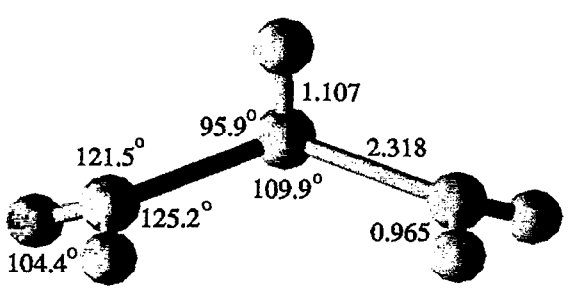

FIG. 6. The optimized geometry of $NO^+(H_2O)_2$ predicted at the MP2/6-31G** level. In the calculation, the geometry of the cluster was constrained to C_s symmetry. Bond lengths are in Å.

The CCSD binding enthalpy calculated at the MP2/6-31G** level (Table VII) is 17.5 kcal mol^{-1}, in good agreement with the value of 16.1±1.0 kcal mol^{-1} measured by French *et al.*[9] The predicted OH stretch spectrum consists of the symmetric and antisymmetric H_2O bands at scaled frequencies of 3623 and 3706 cm^{-1} with similar intensities.

V. DISCUSSION

A. Protonated nitrous acid, $NO^+(H_2O)$

The experimental results on the $n=1$ cluster are most consistent with the structure of a weakly bound ion–molecule complex, $NO^+(H_2O)$. We find that photodissociation of protonated nitrous acid leads to $NO^+ + H_2O$ products. The frequency of the observed vibrational band, 3605 cm^{-1}, agrees within 5% of the scaled MP2 frequency of the H_2O symmetric stretch, 3587 cm^{-1}. However, we do not observe an antisymmetric stretch band, which our calculations predict would occur at 3671 cm^{-1} (scaled) with an intensity 80% of that of the symmetric stretch.

From the quadratic fluence dependence, we find that dissociation requires at least two photons, placing a lower limit of 10.3 kcal mol^{-1} on the $NO^+\cdots(H_2O)$ binding energy. This lower bound is consistent with the dissociation enthalpy measured by French *et al.*[9] of 18.5±1.5 kcal mol^{-1}, and with our CCSD estimate of the dissociation enthalpy, $\Delta H^\circ_{298}=20.9$ kcal mol^{-1}. Our result places a lower bound on the proton affinity of nitrous acid of PA≥179.5 kcal mol^{-1}, consistent with the theoretical value of PA=187 kcal mol^{-1} calculated by De Petris *et al.*[17]

The O═N···O angle predicted by the MP2/6-31G** calculation is sharply bent, and the water molecule is oriented with a lone pair pointed towards the N atom. This geometry can be understood as the lone pair electrons of the O atom of H_2O donating density into the empty π^* orbitals of NO^+, which have significant *p* character on the N atom.

The *ab initio* structure for $NO^+(H_2O)$ is a near prolate top with rotational constants of $A=1.96$ cm^{-1}, $B=0.239$ cm^{-1}, and $C=0.219$ cm^{-1}, yielding an asymmetry parameter of $\kappa=-0.977$. Using this calculated geometry, we can simulate the rotational envelope of the H_2O symmetric stretch band. The symmetry axis of the H_2O moiety is approximately collinear with the *a* axis of the cluster; therefore,

excitation of the symmetric H_2O stretch will result in approximate a-type selection rules. We have modeled the rotational contour by deriving a predicted rovibrational spectrum for a semirigid rotor and then convoluting it with a Gaussian linewidth function. We used centrifugal distortion constants and differences between upper and lower state constants similar to those in HONO,[28] although the $NO^+(H_2O)$ complex will be floppier. Figure 5 compares the observed band contour with a simulation of the rovibrational spectrum at a rotational temperature, 120 K, convoluted with our laser linewidth of 1.5 cm^{-1}. This temperature is realistic, given that we have successfully fit a spectrum of SiH_7^+ clusters formed in the same source using 90 K.[20] Both the width of the band and the doublet shape and splitting are well simulated. The relatively narrow width of the band can only be simulated by an a-type transition. The doublet structure stems from the P and R branches, with the relatively weak Q branch blending into the P branch. The band intensity is weighted towards the P branch, indicating that the rotational constant $\frac{1}{2}(B'+C')$ increases slightly in the upper state. Such a change can occur if the O=N···O angle decreases slightly upon excitation. In summary, the rotational contour is consistent with both the predicted rotational constants and selection rules, and provides further confirmation in support of the proposed structure.

The only discrepancy between the experimental results and the proposed structure is the absence of the antisymmetric stretch in the experimental spectrum. Our *ab initio* calculations predict that in $NO^+(H_2O)$, both OH stretch bands have intensities considerably enhanced over those in neutral H_2O. However, the antisymmetric band intensity, normally significantly stronger than that of the symmetric stretch, is calculated to be slightly weaker.

An explanation for the observation of only one OH stretch band is that the structure is the covalently bound $N(OH)_2^+$ [Fig. 1(b)], for which the two OH vibrations are nearly degenerate. We discount this possibility for several reasons. First, it is unlikely that this isomer is formed. $N(OH)_2^+$ is calculated to be a highly energetic metastable lying ΔE_0=32.7 kcal mol^{-1} above the ion–molecule complex. Previous experiments find no evidence for this isomer in flow tubes, stationary afterglows, and high-pressure discharges. Our source is also a high-pressure discharge with the plasma occurring in a narrow channel followed by supersonic expansion, and the chemistry is similar. Second, in order for two-photon excitation to dissociate $N(OH)_2^+$, an intramolecular hydrogen atom transfer over two atoms, from one O atom to the other, must occur followed by cleavage of the $NO^+\cdots(OH_2)$ bond. The barrier for what is essentially a 1,3 hydrogen shift must be less than 21 kcal mol^{-1}. Third, our MP2 calculations predict that the OH stretches for this isomer are not actually degenerate, but are rather split by 50 cm^{-1}. Furthermore, the scaled OH symmetric and antisymmetric stretching frequencies of $N(OH)_2^+$ are predicted at 3390 and 3338 cm^{-1}, respectively, i.e., more than 200 cm^{-1} below the observed transition, and thus disagree with experiment.

Similar reservations apply to the covalent structure formed by protonating the nitrogen atom, $HON(H)O^+$. This isomer is predicted to be ΔE_0=35.8 kcal mol^{-1} above the $NO^+(H_2O)$ energy, and it can only dissociate to $NO^+ + H_2O$ following isomerization by a hydrogen shift. The barrier for this shift, with the proton bridging an N—O sigma bond, is also likely to be high. Furthermore, our calculations predict that there will be two bands in the region scanned, the OH and NH stretches, both having scaled frequencies 280 cm^{-1} or more to the red of the observed band.

The reason for the absence of an antisymmetric H_2O stretch absorption may lie in the fact that the spectra are not absorption spectra, but rather two-photon dissociation spectra. A discrepancy can come about if (a) the multiphoton absorption process is highly inefficient for ν_3 relative to ν_1 absorption, or (b) clusters excited in this mode do not efficiently dissociate.

There is a physical basis for a larger two-photon absorption cross section for the ν_1 absorption. Multiphoton absorption occurs either by sequential absorption, e.g., $0\rightarrow\nu_3\rightarrow 2\nu_3$, or nonresonantly via an intermediate virtual state. In the free H_2O monomer, the anharmonicity constants[33] are $x_{11}=-43$ cm^{-1}, $x_{13}=-155$ cm^{-1}, and $x_{33}=-46$ cm^{-1}. Thus, the $\nu_1\rightarrow 2\nu_1$ and $\nu_3\rightarrow 2\nu_3$ transitions are off-resonance from the fundamentals by over ~170 cm^{-1}. However, the $\nu_1\rightarrow\nu_1+\nu_3$ transition is at 3600 cm^{-1}, close to the ν_1 frequency of 3657 cm^{-1}. Thus, two-photon excitation of the symmetric stretch will be far more efficient because the second photon can excite the red-shifted antisymmetric stretch hot band transition. The $0\rightarrow\nu_1\rightarrow\nu_1+\nu_3$ process is therefore a near-resonant two-photon process. While the frequencies differ in the $n=1$ cluster, this effect should still be qualitatively correct. Thus, two-photon dissociation was observed for ν_1, while the ν_3 band was too weak to be detected experimentally. We plan to test this hypothesis in a two-color photodissociation experiment.

The weakness of two-photon ν_3 absorption is also consistent with the appearance of the antisymmetric stretch band in all larger hydrates of NO^+ and its increases in intensity with cluster size relative to the ν_1 band. As discussed in Sec. V B, this result can be explained if the ν_3 signal in the larger clusters arises from one-photon dissociation.

The absence of a band due to the ν_3 vibration could also arise because this mode relaxes more slowly than ν_1. The ν_3 mode has A'' symmetry and will be not be as strongly coupled to the intermolecular stretch as the ν_1 mode, which possesses A' symmetry. The differences in coupling could then lead to variations in predissociation rates. If clusters prepared by exciting the ν_3 band predissociate with lifetimes greater than ~10 μs, they would be undetected. Alternatively, relaxation rates could affect the observed action spectra if two-photon absorption takes place by the following three-step process: excitation of a $0\rightarrow 1$ transition, intramolecular vibrational relaxation (IVR) of the O–H stretch, and subsequent reexcitation of the $0\rightarrow 1$ transition of the hot cluster. If IVR from the ν_3 levels occurs on time scales longer than the laser pulsewidth (10^{-8} s), the second photon would not be absorbed, and no dissociation would occur. IVR from ν_1 mode must then occur at rates faster than 10 ns to account for the observed band. This possibility could be tested by exciting clusters at ν_3 with two pulses separated by ~100 ns.

B. $NO^+(H_2O)_n$, $n=2$ and 3

The predissociation spectra and the photoproducts of $NO^+(H_2O)_n$ ($n=2$ and 3) suggest that these clusters also have water ligands bound to an NO^+ ion core. Unlike the $n=1$ cluster, both symmetric and antisymmetric stretch bands are observed. These vibrations gradually shift to higher frequencies with cluster size in going from $n=1$ to 3 (Fig. 3), as expected for the increasing hydration of the NO^+ ion core.

The reduction in binding energy with n is also evident in the fluence dependence of the photodissociation yield when exciting the ν_1 band. This dependence can be either linear or nonlinear for $n=2$, and becomes linear for $n=3$. In the $n=2$ case, the photon energy is less than the cluster dissociation energy and the linear dependence arises from dissociation of vibrationally hot ions. When the distribution is cold, then signal from two-photon dissociation is comparable to one-photon dissociation of a smaller population of vibrationally hot complexes, resulting in both linear and quadratic contributions to the fluence dependence. When the distribution is hotter, one-photon dissociation dominates.

In the *ab initio* structure of the $n=2$ complex, the water ligands both bind to the nitrogen atom of the NO^+, as in $n=1$. The N=O bond is directed almost perpendicular to the ONO plane, indicating that the water molecules again interact with the p orbitals of the N atom, one H_2O donating lone pair density into the π_x^* orbital, the other into the π_y^* orbital.

The $n=3$ spectrum indicates that all three H_2O are equivalent, and a postulated structure for $NO^+(H_2O)_3$ is shown in Fig. 7(a). The third H_2O also binds to the N atom of NO^+, with a lone electron pair of each of the H_2O molecules again donating into the π^* orbital. We expect that the three water ligands will be symmetrically positioned about the ion.

The H_2O antisymmetric stretch transitions appear as broad features that grow in intensity with cluster size relative to the narrower symmetric stretch band. Indeed, there appears to be a progression from a complete absence in $n=1$, to a relatively weak shoulder in $n=2$, to a strong band in $n=3$. This result can be understood if the ν_3 signal primarily arises from one-photon dissociation of vibrationally excited clusters. For the $n=1$ cluster, few of the ions are hot enough to dissociate after absorption of a single photon and no ν_3 band is observed. For the $n=2$ cluster, the H_2O binding energy is 2.4 kcal/mol^{-1} lower and a detectable fraction of the clusters is able to dissociate upon absorption of a photon. The ν_3 dissociation signal becomes even larger for $n=3$, since the binding energy decreases and the total internal energy increases with the increase in cluster size. Alternatively, if the absence of the ν_3 band is due to low predissociation rates, this effect could arise from the decreases in predissociation lifetime with n.

C. $NO^+(H_2O)_4$ and opening of the reactive channel

The observed spectrum (Fig. 3) of the $n=4$ cluster suggests that this complex is also comprised of water ligands bound to an NO^+ core; however, the fourth water ligand does not apparently bind directly to the NO^+ cation. The appearance of bands at 3375 and 3230 cm^{-1} indicate that hydrogen bonds have formed and that the fourth H_2O binds to the other water ligands, beginning a second solvation shell. Below, we discuss several plausible solvent configurations.

The simplest configuration involves the fourth water forming a hydrogen bond with one of the first shell H_2O molecules, as depicted in Fig. 7(b). The binding energy for a second shell H_2O should be on the order of 6–10 kcal mol^{-1}, and thus will be comparable to the estimated energy for binding a fourth water ligand directly to the NO^+ core. The dissociation channel leading to loss of two H_2O molecules can then be understood as evaporation of $(H_2O)_2$, with a first solvation shell water carrying along its second shell partner. However, this configuration will give rise to only one hydrogen-bonded OH absorption band.

Small water clusters are well known for forming cyclic structures in order to maximize stabilization by hydrogen bonding.[34] The second shell energy would be more favorable if the fourth H_2O could form hydrogen bonds with two H_2O ligands, as depicted in Fig. 7(c). In this structure, the water bridges two adjacent ligands to form a ring of four heavy atoms (three water O atoms and the N^+). If we assume that the $H_2O\cdots N\cdots OH_2$ angle is 120° and the N···O bond length is 2.4 Å (slightly longer than calculated for $n=2$), the separation between O atoms on the H_2O ligands is 4.2 Å, comparable to the 4.48 Å distance in ice. The hydrogen-bonded rings in ice I are six-membered, but tetrahedral structures similar to those proposed here exist in ice VI. The strain will be lower in the unconstrained cluster, because the soft N···O stretches and O···N···O bend allow the cluster to readily deform. By forming two hydrogen bonds, the second shell H_2O should bind by at least 6–10 kcal mol^{-1}. This structure should be at least comparable in stability to having four waters in the first shell. The bands observed at 3230 and 3375 cm^{-1} could then be assigned as symmetric and antisymmetric stretch modes of the two hydrogen-bonded OH bonds.

An alternative structure, shown in Fig. 7(d), consists of the adducts of the reaction products, with a HONO molecule and two H_2O bound to a central hydronium ion core. This structure is not in accord with the observed spectrum. The hydronium ion OH bonds would all be red-shifted below 2700 cm^{-1}, and thus unobserved. The two bands above 3600 cm^{-1} can be assigned to the H_2O molecules, but the 3375 and 3230 cm^{-1} bands cannot be accounted for. Furthermore, an OH stretch band of the HONO ligand is not observed.

The structure we propose in Fig. 7(d) is topologically equivalent to the structure proposed by Fehsenfeld *et al.*[6] [shown in Fig. 7(e)]. This structure was suggested as an intermediate in reaction (1) from $NO^+(H_2O)_3+H_2O$ to $H_3O^+(H_2O)_2+HONO$. They proposed that one (first shell) H_2O was bound to NO^+, with a single H_2O in turn bound to that. The remaining two H_2O molecules were in the third shell, hydrogen-bonded to the second shell H_2O. This structure is more consistent with our observed spectrum, since there are three hydrogen-bonded OH groups, as well as two H_2O ligands with free OH groups. If the charge remains localized on the N atom, however, this configuration will be highly energetic, and unlikely to be formed.

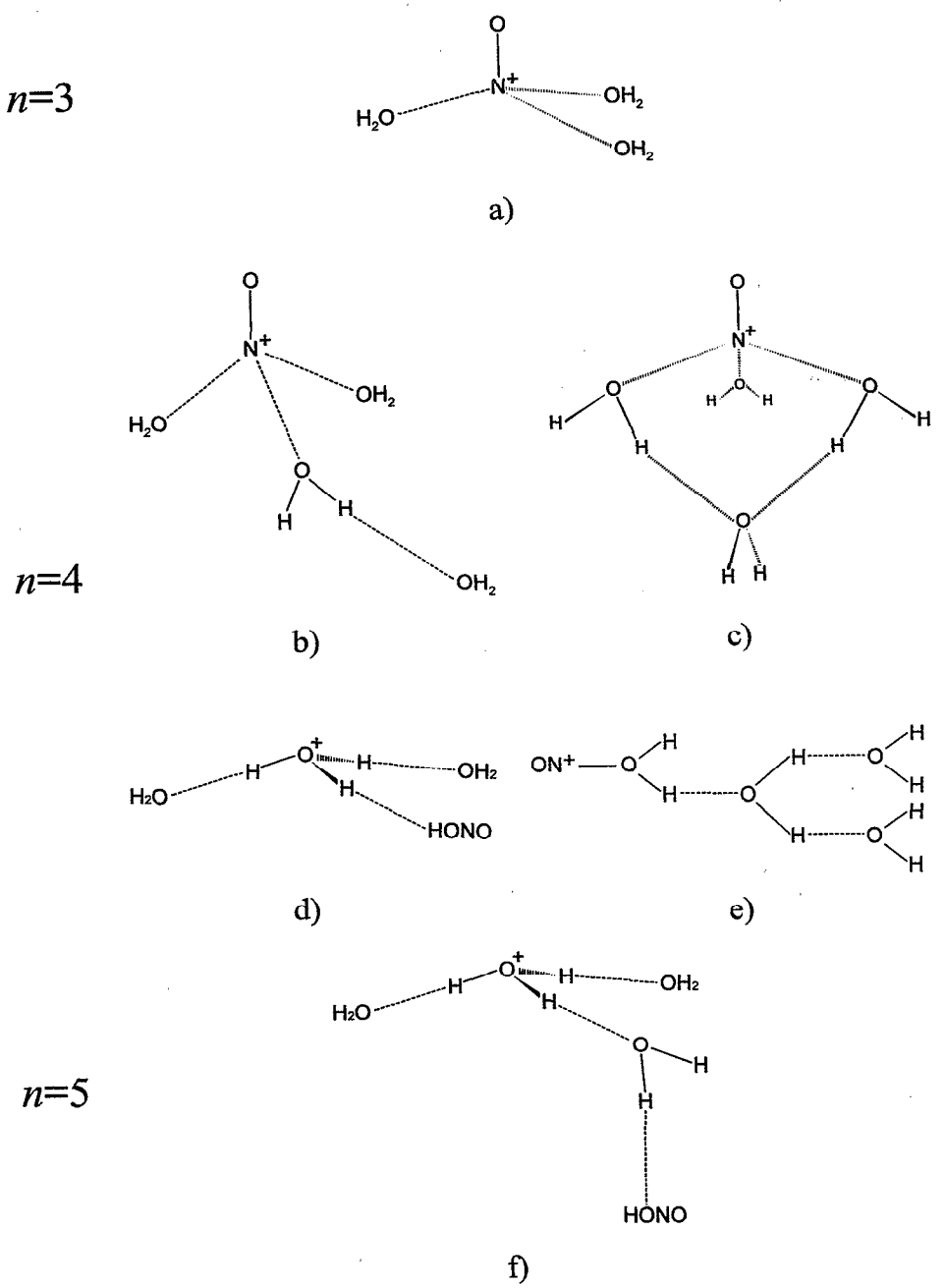

FIG. 7. Proposed structures of the nitrosonium ion hydrates $NO^+(H_2O)_n$, for $n=3$ to 5.

Fehsenfeld *et al.* also proposed a "linear" structure, in which the four H_2O molecules form a single hydrogen-bonded chain with the O atom on a terminal water binding to the NO^+:

$$ON^+ \cdots O(H)-H \cdots O(H)-H \cdots O(H)-H \cdots O(H)-H.$$

This structure is not consistent with the observed spectrum. We would expect to observe a progression of three hydrogen-bonded OH stretches of increasing red-shift and intensity, and the ν_1 band of H_2O should be significantly weaker, since only one water molecule is not a donor. Such a structure, while possibly a local energy minimum, is also energetically unfavored. Two of the water molecules are over 7 Å from the charge, and will contribute little to the solvation energy. Furthermore, if we postulate a structure in which HONO is formed and a proton is transferred to the second H_2O to form H_3O^+, ~5–10 kcal mol^{-1} are lost in having the last water in a second shell position, making the reaction significantly endothermic.

From the observation of HONO products in the absence

of a HONO absorption band, we conclude that one IR photon can induce the reaction

$$NO^+(H_2O)_4 \rightarrow H_3O^+(H_2O)_2 + HONO. \quad (4c)$$

French *et al.*[9] estimate that the two channels, loss of H_2O (4a) and loss of HONO (4c), are almost identical in energy, but we find that the yield of HONO is significantly lower (10%). There are several plausible reasons why unimolecular decay of excited $NO^+(H_2O)_4$ favors H_2O loss. First, the estimated dissociation energies are comparable to the photon energy; if the molecule is excited close to threshold, differences of even a few kcal mol^{-1} can greatly influence the branching ratio. Second, the reaction (4c) may have an activation energy significantly larger than the H_2O binding energy, $E_{act}>10$ kcal/mol. A barrier between $NO^+(H_2O)_4$ and $H_3O^+(H_2O)_2$(HONO) is plausible, especially if the solvent H_2O must rearrange as the charge is transferred. Finally, unimolecular decay via the reactive channel may also be limited by the entropy of activation. Evaporation of H_2O from $NO^+(H_2O)_4$ proceeds by simple bond fission, but formation of HONO may occur by a concerted reaction. In particular, substantial solvent rearrangement within the cluster may inhibit the reaction even if the HONO channel is energetically accessible.

D. The $n=5$ cluster: $H_3O^+(H_2O)_3$(HONO)

The large differences in the spectrum of $n=5$ compared to the spectra of the smaller clusters signal a qualitative change in the nature of the clusters. The broad, strong absorption band near 2800 cm^{-1} and the weaker band at 3190 cm^{-1}, which we assigned as the OH stretches of H_3O^+, provide clear evidence that the $n=5$ complex has an H_3O^+ ion core hydrogen-bonded to three solvating ligands. The appearance of the higher-frequency bands of the $n=5$ cluster is also distinct, with several sharp bands instead of the pattern of a sharp ν_1 and broad ν_3 bands observed in the smaller clusters. Because HONO is the dominant dissociation product, we infer that HONO forms weaker hydrogen bonds than H_2O. We thus propose that the $n=5$ clusters have the structure shown in Fig. 7(f), with the H_3O^+ bound to three water molecules in the first solvation shell and a HONO molecule in the second shell hydrogen-bonded to one of the first shell waters.

Given this structure, we can assign the five bands observed in the 3500 to 3800 cm^{-1} region (shown in more detail in Fig. 8). We distinguish between the two H_2O ligands which do not act as donors in a hydrogen bond, and the third H_2O ligand, which forms a hydrogen bond with the HONO in the second solvation. The bands at 3644 and 3734 cm^{-1} are close to the free H_2O monomer bands, and are assigned as the symmetric and antisymmetric OH stretches of the two water ligands (not bound to HONO). The third H_2O will have one OH stretch significantly red-shifted, while the other will remain essentially unperturbed. We assign the 3710 cm^{-1} band to the free OH of this perturbed molecule, and the broader band at 3530 cm^{-1} (shifted 125 cm^{-1} from the ν_1 band of the H_2O monomer) to the HO—H···O bond. The remaining band is the sharp, strong feature at 3576 cm^{-1}, 15 cm^{-1} to the red of the *t*-HONO monomer band. We assign this feature as the OH stretch of the nitrous acid ligand.

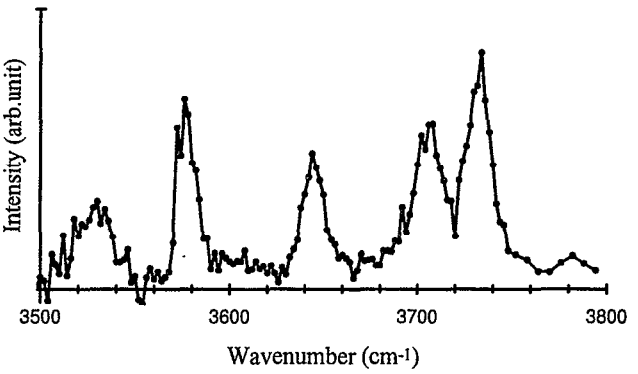

FIG. 8. Details of the vibrational predissociation spectrum of $NO^+(H_2O)_5$ in the 3500–3800 cm^{-1} region. The ordinate is the yield of photofragment ions $H_3O^+(H_2O)_3$.

The frequency of the OH stretch of the nitrous acid ligand suggests that it is the *trans* conformer, since the *t*-HONO monomer stretch has a frequency of 3591 cm^{-1}, while *c*-HONO absorbs at 3426 cm^{-1}.[28] The effect of hydrogen bonding on the OH stretch of HONO is unknown. Thus, the issue of how the HONO is hydrogen-bonded to the cluster (terminal oxygen, N atom, hydroxy group O atom, or bridging) remains uncertain.

E. The intracluster reaction of NO^+

The clusters we observed are intermediate complexes along the pathways for the reaction

$$NO^+(H_2O)_{n-1} + H_2O \rightarrow H_3O^+(H_2O)_{n-2} + HONO. \quad (6)$$

The energetics along the reaction coordinates for $n=2$–5 are illustrated in Fig. 9. From their hydration enthalpy measurements, French *et al.*[9] show that the reaction is endothermic for $n=2$ and 3 by 23.6 and 8.1 kcal mol^{-1}, respectively. Using their estimated value of $\Delta H_{2,3}$, the reaction for $n=4$, i.e., reaction (1), is slightly endothermic (~2 kcal mol^{-1}). If we continue their extrapolation, then $\Delta H_{3,4}$ is ~10 kcal mol^{-1}, and we estimate that the reaction enthalpy for $n=5$ is −6 kcal mol^{-1}.

Our results are consistent with the thermodynamics. For reactions which are endothermic ($n\leq 4$), the complexes we observed are adducts of the reactants NO^+ and H_2O. The structure of the $n=5$ cluster, $H_3O^+(H_2O)_3$(HONO), reflects the fact that the reaction for $n=5$ is exothermic. Although the cluster $NO^+(H_2O)_5$ may be stable, it is probably higher in energy than the observed cluster (see Fig. 9).

While the reaction goes to completion for five water molecules, we find evidence for the onset of reaction in the $n=4$ cluster, even though the reaction is probably endothermic. Absorption of one IR photon (~10.5 kcal mol^{-1}) leads to ~12% yield of HONO formation. The photon energy is approximately equal to the internal energy of the activated complex formed in the thermal collision $NO^+(H_2O)_3+H_2O$. Thus, we would expect that such collisions would lead to reaction approximately 10% of the time. This reaction effi-

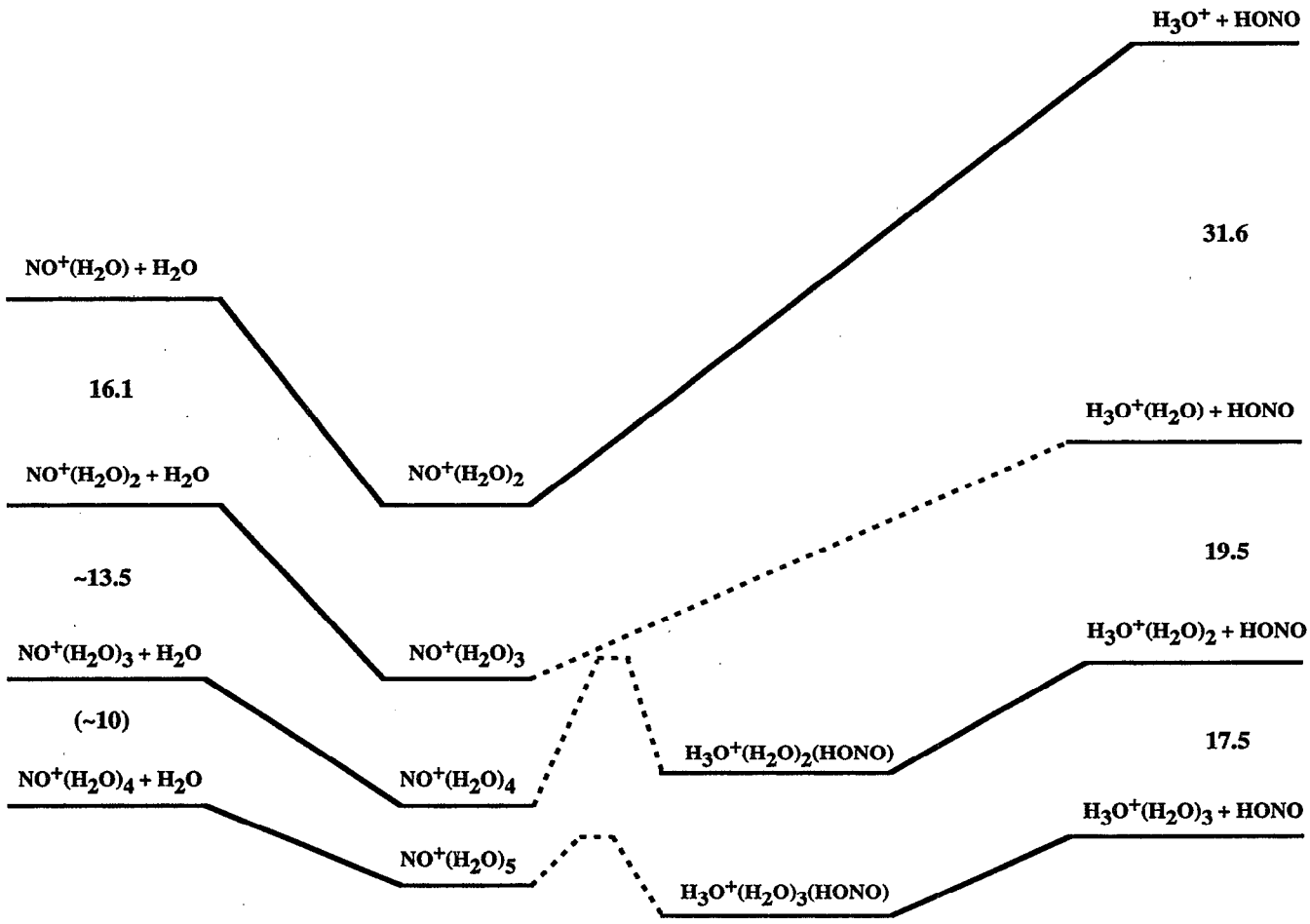

FIG. 9. Energy level diagram for the reactions $NO^+(H_2O)_{n-1}+H_2O \rightarrow NO^+(H_2O)_n \rightarrow H_3O^+(H_2O)_{n-2}+HONO$. Dashed lines indicate hypothesized reaction paths and transition states. Each reaction pathway for a cluster n is lowered relative to the $n-1$ pathway by the hydration enthalpies. Numbers are hydration enthalpies in kcal mol^{-1}; those in parentheses are estimates only.

ciency is consistent with the observed rate constant, 7×10^{-11} $cm^3\ s^{-1}$, which is about one order of magnitude lower than the rate constant for ion–dipole collisions.

In the earlier static and flow tube experiments, $NO^+(H_2O)_4$ was not observed. This can be understood since the reaction rate is greater than three-body stabilization of the adduct. Furthermore, once $H_3O^+(H_2O)_2$ is formed, it quickly equilibrates to form larger hydrates. The backreaction is inhibited by the reduced concentration of $H_3O^+(H_2O)_2$ and the negligible concentration of HONO.

Reorganization of the H_2O molecules is almost certainly required for the reaction to proceed, because the charge is transferred from the nitrogen atom to an H_3O^+ moiety. The barrier for this process is still relatively high in $n=4$, but is readily overcome in $n=5$. Additional experiments on the $n=4$ cluster, aided by computational studies, may provide further insights into the activation steps of this reaction.

VI. SUMMARY

Our results provide clear evidence for a rearrangement of $NO^+(H_2O)_n$ at larger cluster sizes. The experimental results indicate that the smaller clusters are nitrosonium ions bound by water ligands and are in accord with the theoretical calculations for $n=1$ and 2. The cluster $n=4$, however, begins to deviate from this picture with the appearance of new hydrogen-bonded OH stretch absorptions and the opening of a minor photodissociation channel giving rise to loss of HONO. This behavior presages the large changes in the vibrational spectrum and photodissociation behavior observed after adding a fifth water molecule. The $n=5$ cluster forms an adduct of the reaction products, $H_3O^+(H_2O)_3(HONO)$.

ACKNOWLEDGMENTS

We acknowledge support of an NSF Presidential Young Investigator Award No. CHEM-8957423, E. I. DuPont de-Nemours and Company, the Irvine Foundation, the Chevron Fund, an AT&T Special Purpose Grant, an NSF predoctoral fellowship for K. T. K., and the JPL Supercomputer Project for the computational studies. We are grateful to Mary Frances Jagod for her heroic efforts in reprogramming the asymmetric rotor spectrum prediction program ASMWIR, and to the Materials and Molecular Simulations Center of the Beckman Institute for the graphics facilities used in generating Fig. 6.

[1] E. E. Ferguson, F. Fehsenfeld, and D. L. Albritton, in *Gas Phase Ion Chemistry*, edited by M. T. Bowers (Academic, New York, 1979); G. Brasseur and S. Solomon, *Aeronomy of the Middle Atmosphere* (Reidel, Dordrecht, Holland, 1986).
[2] R. S. Narcisi and A. D. Bailey, J. Geophys. Res. **70**, 3687 (1965).
[3] F. C. Fehsenfeld and E. E. Ferguson, J. Geophys. Res. **74**, 2217 (1969).
[4] W. C. Lineberger and L. J. Puckett, Phys. Rev. **187**, 286 (1969).
[5] L. J. Puckett and M. W. Teague, J. Chem. Phys. **54**, 2564 (1971).
[6] F. C. Fehsenfeld, M. Mosesman, and E. E. Ferguson, J. Chem. Phys. **55**, 2120 (1971).
[7] C. J. Howard, H. W. Rundle, and F. Kaufman, J. Chem. Phys. **55**, 4772 (1971).
[8] L. J. Puckett and W. C. Lineberger, Phys. Rev. A **1**, 1635 (1970).
[9] M. A. French, L. P. Hills, and P. Kebarle, Can. J. Chem. **51**, 456 (1973).
[10] N. A. Burdett and A. N. Hayhurst, J. Chem. Soc. Faraday Trans. 1 **78**, 2997 (1982).
[11] S. Patai, *The Chemistry of Amino, Nitroso, and Nitro Compounds and Their Derivatives* (Wiley, New York, 1982), and references therein.
[12] M. J. S. Dewar, M. Shanshal, and S. D. Worley, J. Am. Chem. Soc. **91**, 3590 (1969).
[13] K. A. Jorgensen and S. O. Lawessen, J. Chem. Soc., Perkin Trans. 2 **1985**, 231.
[14] A. Dargelos, S. El Ouadi, D. Liotard, M. Chaillet, and J. Elguero, Chem. Phys. Lett. **51**, 545 (1977).
[15] W. D. Edwards and H. Weinstein, Chem. Phys. Lett. **56**, 582 (1978).
[16] M. T. Nguyen and A. F. Hegarty, J. Chem. Soc., Perkin Trans. 2 **1984**, 2037.
[17] G. De Petris, A. D. Marzio, and F. Grandinetti, J. Phys. Chem. **95**, 9782 (1991).
[18] H. M. Rosenstock, K. Draxl, B. W. Steiner, and J. T. Herron, J. Phys. Chem. Ref. Data **6**, Supp. 1 (1977).
[19] M. Okumura, L. I. Yeh, J. D. Myers, and Y. T. Lee, J. Phys. Chem. **94**, 3416 (1989); L. I. Yeh, M. Okumura, J. D. Myers, J. M. Price, and Y. T. Lee, J. Chem. Phys. **91**, 7139 (1989); J. M. Price, Ph.D. thesis, University of California at Berkeley (1990); J. M. Price, M. W. Crofton, G. Neidenauer, and Y. T. Lee, J. Phys. Chem. **95**, 2182 (1991).
[20] Y. Cao, J.-H. Choi, B.-M. Haas, M. S. Johnson, and M. Okumura, J. Phys. Chem. **97**, 5215 (1993).
[21] W. L. Liu and J. M. Lisy, J. Chem. Phys. **89**, 605 (1988).
[22] *Ion and Cluster Ion Spectroscopy and Structure*, edited by J. P. Maier (Elsevier, Amsterdam, 1989).
[23] Y. Cao, J.-H. Choi, B.-M. Haas, M. S. Johnson, and M. Okumura, J. Chem. Phys. **99**, 9307 (1993).
[24] Y. Cao, B.-M. Haas, J.-H. Choi, and M. Okumura (to be submitted).
[25] S. J. Brosnan and R. L. Byer, IEEE J. Quantum Electron. **QE-15**, 415 (1979).
[26] G. Herzberg, *Molecular Spectra and Molecular Structure. III. Electronic Spectra of Polyatomic Molecules* (van Nostrand Reinhold, New York, 1966).
[27] H. A. Schwarz, J. Chem. Phys. **67**, 5525 (1977).
[28] C. M. Deeley and I. M. Mills, J. Mol. Struct. **100**, 199 (1983); S. M. Holland, R. J. Stickland, M. N. R. Ashfold, D. Z. Newnham, and I. M. Mills, J. Chem. Soc., Faraday Trans. **87**, 3461 (1991).
[29] M. E. Jacox, J. Phys. Chem. Ref. Data **19**, 1387 (1990).
[30] C. Møller and M. S. Plesset, Phys. Rev. **46**, 618 (1931).
[31] W. J. Hehre, R. Ditchfield, and J. A. Pople, J. Chem. Phys. **56**, 2257 (1972); P. C. Hariharan and J. A. Pople, Theor. Chim. Acta. **28**, 213 (1973).
[32] M. J. Frisch, G. W. Trucks, M. Head-Gordon, P. M. W. Gill, M. W. Wong, J. B. Foresman, B. G. Johnson, H. B. Schlegel, M. A. Robb, E. S. Replogle, R. Gomperts, J. L. Andres, K. Raghavachari, J. S. Binkley, C. Gonzalez, R. L. Martin, D. J. Fox, D. J. DeFrees, J. Baker, J. J. P. Stewart, and J. A. Pople, GAUSSIAN 92, Revision D, Gaussian, Inc., Pittsburgh, PA, 1992.
[33] G. Herzberg, *Molecular Spectra and Molecular Structure. II. Infrared and Raman Spectra of Polyatomic Molecules* (van Nostrand Reinhold, New York, 1945).
[34] See, for example, S. S. Xantheas and T. H. Dunning, J. Chem. Phys. **99**, 8774 (1993).